Philippine Journal of Science
153 (4): 1329-1343, August 2024
ISSN 0031 - 7683
Date Received: 16 Aug 2023

Fabrication of a Concrete Roof Tile by Geopolymerization of Red Clay with Container Glass Wastes

Keith T. Bulaybulay[1], Jessel Grace L. Orpeza[2], and Ruben L. Menchavez[3]*

[1]Technical Development, TECDIA Cebu Inc.,
Mactan Export Processing Zone, Lapu-Lapu City, Cebu, 6016 Philippines
[2]Ceramic Wafer Process, TECDIA Cebu Inc.,
Mactan Export Processing Zone, Lapu-Lapu City, Cebu, 6016 Philippines
[3]Department of Materials and Resources Engineering and Technology,
College of Engineering, Mindanao State University–Iligan Institute of Technology,
Tibanga, Iligan City, 9200 Philippines

We report the production of concrete roof tiles using a red clay-based geopolymer binder with container glass waste and river sand as a concrete filler. Clear and colored container glass wastes were separately ground to powder and blended with low-grade red clay to achieve a SiO_2/Al_2O_3 ratio of approximately 7.0. The powder blends were converted to geopastes with a solid-to-alkali solution ratio of approximately 0.8 using a 12-molar alkali activator solution containing a mixture of potassium hydroxide and sodium hydroxide. Rheological analysis showed that the geopaste binders with transparent and colored glass powders exhibited high shear thinning behavior. A higher viscosity was observed for the geopaste with colored glass powder due to the presence of colorants. Fine and coarse particles of river sand were prepared and mixed with different ratios of geopaste binder to river sand of 1:2.0, 1:2.5, and 1:3.0, respectively. All geopaste and river sand formulations were poured into acetate molds and heated in a metal chamber at 80 °C for 24 h, then aged at room temperature for 14 d. The highest flexural strength of 2.33 MPa was obtained from the formulation with a 1:2 ratio of geopaste with transparent glass powder and fine sand. The measured strength corresponded to an apparent porosity of 6.30% and a water absorption of 4.50%. The bulk density was approximately 1.16 g/cm³, which is classified as a lightweight material. A prototype geopolymer concrete roof tile was successfully produced with a sorption coefficient of approximately 0.170 mm/min$^{1/2}$. This measured sorption coefficient and the physical properties indicate that the produced roof tile is a potential building material.

Keywords: alkali activator, container glass, geopolymer, red clay, roof tile, waste

INTRODUCTION

Concrete-based tiles have long been the preferred roofing material for residential buildings due to their impressive durability, fire, and water resistance, as well as low maintenance requirements. They are classified as exterior building materials that are also energy efficient, providing a comfortable indoor environment in cold and warm climates at a lower cost than other roofing materials (Qin *et al.* 2017). This type of roofing material is usually mass-produced by filling mold cavities with typical concrete mixes of different sizes of sand aggregate, water, and cement binder. However, using cement binders in concrete products presents the dilemma of a relatively large carbon footprint in cement production, as the conversion of precursor raw materials is a highly endothermic process

*Corresponding author: ruben.menchavez@g.msuiit.edu.ph

(Martínez-Martínez *et al.* 2023). Therefore, there is a growing interest in finding a concrete binder with minimal environmental impact at a reasonable cost.

Geopolymer technology offers a promising solution for producing exterior building materials with desirable physical properties while reducing environmental impact (Morsy *et al.* 2014). The term "geopolymer," coined by Davidovits, refers to a cementitious material that uses silica and alumina in a highly alkaline solution. Alkaline activation of both oxides occurs during curing to develop an inorganic polymer with three-dimensional alumino-silicates. The required oxides can be provided by waste materials ranging from raw kaolinitic clays to industrial inorganic wastes. Natural kaolinitic clay is usually heat treated at high temperatures to obtain an alkaline reactive metakaolin phase, whereas the inorganic waste can be used as is with minimal processing. Several studies have been published elsewhere declaring the compatibility of the geopolymer binder with sand aggregates to produce concrete-based products (Singh *et al.* 2015). Other inorganic wastes can fully or partially replace the geopolymer binder's components and aggregates.

Glass waste is another type of inorganic waste, mainly rich in silica and minor oxides. Most of this waste comes from mass-produced glass, known as industrial glass, and a small percentage comes from non-industrial glass such as that used in medical, automotive, optical, and electronic applications. Industrial glass accounts for 95% of glass production volume and includes flat glass, container glass, fiberglass, and utility glass. On the other hand, non-industrial glasses tend to be expensive because they are melted with high-purity precursors in very small quantities to provide specific properties for a demanding application. It is worth noting that most types of glass are highly resistant to chemical attack by chemical substances. Despite the chemical durability of glass, it is still susceptible to attack by strong acid and alkaline solutions with different modes and degrees of corrosion (Douglas and El-Shamy 1967), depending on its chemical composition. This corrosion behavior is required in the geopolymer reaction, which mainly involves the dissolution of aluminosilicate precursors in highly alkaline solutions. It has been reported that the amorphous silica in glass waste is readily dissolved in a strong alkaline solution at pH above 10.7 to form leachable silicate (Conradt 2008). For faster geopolymerization, the glass-loaded geopaste is usually heated to a high temperature of about 80 °C to increase the solubility of the glass (Goto 1955). Some promising studies on the use of non-industrial glasses in geopolymers have been described in the literature (Gao *et al*. 2022; Novais *et al*. 2016; Lo *et al*. 2018). However, industrial glasses in the form of container glasses represent potential waste resources.

Container glass refers to all types of glass bottles and jars used to store beer, wine, beverages, pharmaceuticals, perfumes, and food products. This type of glass is transparent and colored, depending on the product to be contained. The colored glasses are usually obtained by adding essential colorants such as iron oxide, sulfate, and carbon, which protect the product from deterioration due to ultraviolet radiation. With such a wide range of bottled products, glass bottle waste accounts for approximately 80% of the total glass waste generated. As little as 10–30% of the recycled glass is used as feedstock for the production of new glass bottles, leaving large surpluses for other alternative uses (Siddika *et al*. 2021). Recycling of glass bottles has been reported elsewhere as a primary or partial component of aluminosilicate precursors in geopolymer pastes for concrete applications (Hamzah *et al*. 2021; Maraghechi *et al*. 2014). The powdered form of this glass has been successfully blended with slag, fly ash, and metakaolin to form geopolymer products (Manikandan and Vasugi 2022), but the combination with other aluminosilicate waste resources has not provided a viable forming route.

The route of geopolymer formation from reddish inorganic wastes – including red mud (Vafaei *et al*. 2021), mining waste, and waste-fired bricks (Toniolo *et al*. 2017) – has been successfully reported elsewhere as aluminosilicate precursors containing significant amounts of iron oxide. These reddish wastes are prepared in combination with transparent, colored, or a mixture of these waste glasses – each of which has been studied as a binder in geopolymer products. However, access to these inorganic wastes is difficult everywhere, and a natural red clay deposit is a readily available option for geopolymer precursors. To the best of our knowledge, there is no available literature reporting on the use and comparison of these glass powders in conjunction with impure red clay in geopolymer to produce concrete roofing materials. It is worth noting that red clay provides both silica and alumina with abundant iron oxide and alkali impurities (Raki-in *et al*. 2021). This study addresses this gap by developing geopolymer pastes with impure red clay and type of container glasses (clear and colored) to produce concrete roof tiles. The study has four main objectives: [a] calculate the proportion of aluminosilicate with glass wastes that provide a high silica to alumina ratio, [b] determine the solid loading of aluminosilicate powders containing red clay and type of container glass wastes in alkaline solution based on rheological properties suitable for the workability of concrete mix, [c] optimize the physical properties of the geoconcrete specimens as a function of the geopolymer paste formulation (type of glass powders), the ratio of geopolymer paste to fine aggregate, and the particle size of the fine aggregates, and [d] fabricate prototypes of red clay-based roof tiles using the optimized experimental

conditions and evaluate their fluid sorption performance.

Geopolymerization Process of Concrete Mix

Geopolymer concrete is a mixture of fine aggregates, or a combination of fine and more coarse aggregates, bound together with an aluminosilicate bonding agent. This inorganic binder is readily provided with a variety of inorganic precursors containing silica and alumina oxides, which are reacted with a strongly alkaline solution to produce a strong polymeric product (Shilar *et al*. 2022; Vafaei *et al*. 2021). The reaction product is a geopolymer or binder, composed mainly of amorphous and crystalline phases of zeolitic type, which forms a strong interfacial adhesion on aggregate surfaces (Kai and Dai 2021). The atomic ratio of Si:Al atoms in the aluminosilicate materials determines the type of geopolymer produced. The basic structural subunit is silicon coordinated with four oxygen atoms, and aluminum may replace some of the silicon atoms, depending on the source materials. Geopolymer reactions disrupt the interlinking of the structural subunit with similar tetrahedral units in highly alkaline solutions to yield the amorphous phase. The reaction mechanism generally involves three steps: release of Si and Al atoms from the starting material, formation of Si and/or Si-Al oligomers in solution, polycondensation of the oligomerized species, and binding of the remaining solid particles into the final geopolymeric structure (Dimas *et al*. 2009).

Geopolymeric products (Shilar *et al*. 2023; Cioffi *et al*. 2003) are characterized by the molecular formula $Mn[-(SiO_2)z\text{-}AlO_2)n.wH_2O$ – where M is any alkali cation; z can be 1, 2, or 3; w is the number of water molecules; and n is the extent of polycondensation. The basic monomeric -Si-O-Al - structure is formed with the polysialate unit based on the Si/Al ratio of the aluminosilicates, where the ratio Si/Al = 1 results in the [-Si-O-Al-O] structure. This formula clearly articulates the composition of the geopolymeric products and highlights the importance of the Si/Al ratio in determining the structure of the aluminosilicates. In the poly(sialate-siloxo) structure, which occurs when the Si/Al ratio is 2, the two silicon atoms are in the [-Si-O-Al-O-Si-O-] configuration. On the other hand, when the ratio is 3, the structure involves three Si atoms forming a [-Si-O-Al-O-Si-O-Si-O-] structure. Beyond the ratio of 3, a sialate-linked structure is formed, as observed in silica-based geopolymers (Henao *et al*. 2023; Maraghechi *et al*. 2014).

Although there are several factors that affect the geopolymerization of the dissolved aluminosilicates, the SiO_2/Al_2O_3 ratio plays an important part in enhancing the mechanical properties of the geopolymer. At low Si/Al molar ratios, the initial strength is highly dependent on the amount of Al_2O_3, which makes the geopaste set faster. However, such a lower oxides ratio causes the development of crystalline phases in the hardening geopaste, which are responsible for low-strength products. On the other hand, geopastes with higher SiO_2/Al_2O_3 ratios harden relatively longer. This finding suggests that the Al ions control the solidification time of the geopastes. With a reduced amount of Al ions, the solidification process can be facilitated by thermal treatment. It has been observed that geomaterials with higher SiO_2 to Al_2O_3 ratio have superior strength compared to those with lower SiO_2 to Al_2O_3 ratio (Chindaprasirt *et al.* 2012).

MATERIALS AND METHODS

Starting Raw Materials and Preparations

The red clay used in the experiment was surface-mined from *Barangay* Luinab, Iligan City, Lanao del Norte. The associated moisture was removed in an oven at 110 °C until a constant weight of material was obtained and then pulverized. The ground red clay was screened through 200 mesh (149 μm) and kiln-cured at 800 °C for 5 h. This calcination process was undertaken to secure the formation of the amorphous structure in the red clay (Essaidi *et al*. 2014). The alkaline chemicals such as sodium silicate (water glass: 31.13% SiO_2, 14.65% Na_2O, 51.22% H_2O), sodium hydroxide, and potassium hydroxide were purchased from Joelmar Trading. For the container glass waste, a long-necked Tanduay bottle (750 mL) and a one-liter Red Horse bottle, as shown in Appendix Figure I, were obtained from a local junk shop in Iligan City. They were crushed and oven-dried at 110 °C for 8 h (Toniolo *et al.* 2017). Finally, the fractured glass was reduced to a fine powder using a ball mill.

After the ball milling step, the glass powders were screened through a 200-mesh sieve. On the other hand, the river sand was screened in two separate particle sizes as fine and coarse aggregates. The fine aggregate was prepared by sieving the river sand through a 40-mesh sieve and retaining it on a 60-mesh sieve, and the coarse aggregate was prepared by passing it through a 20-mesh sieve and retaining it on a 40-mesh sieve (Ridtirud and Chindaprasirt 2019). The chemical compositions of the aluminosilicate precursors and river sand were subjected to oxide analyses using an X-ray fluorescence (XRF) analyzer (Olympus Innov-X-DP-6055 Delta).

Preparation of Geopolymer Paste

The geopolymer paste consisted of aluminosilicates and an alkaline solution. The aluminosilicates were a binary mixture of red clay and waste glass. The proportion of each aluminosilicate was calculated based on a molar ratio of

SiO_2/Al_2O_3 greater than the fly ash-based compositions (Dehghani *et al*. 2021) ranging from 3–4.5 and a maximum additive of 20 wt% in the mixture. The calculation required inputting the oxide analyses of the calcined red clay and waste glass powder that were varied from 10–20 wt%. This calculation resulted in two-component powder formulations with codes assigned as F1 (calcined red clay with Tanduay powder) and F2 (red clay with Red Horse powder). The total silica and total alumina in the oxide analysis of the mixtures were each divided by their molecular weights, and their SiO_2/Al_2O_3 molar ratios were reported.

The alkaline solution was prepared at 12 molars (M) by manually dissolving NaOH pellets and KOH flakes in distilled water. The proportions of 75 vol% potassium hydroxide and 25 vol% sodium hydroxide were adapted from a previous study (Alouani *et al*. 2020; Rehman *et al*. 2020). For a small batch of solution containing 62 mL of water, the needed volumes of water for the potassium hydroxide solution were 46.5 mL of water and 15.5 mL of water for sodium hydroxide solution. The respective masses of hydroxides to be prepared to obtain the solution were calculated using Equation 1:

$$(12 \text{ mols} / 1000 \text{ mL}) \times VW \times MW = MH \qquad (1)$$

where VW is the required volume of water, MW is the molecular weight of the hydroxides, and MH is the mass of hydroxides in g. The calculation resulted in 31.3 g of KOH flakes and 7.4 g of NaOH pellets, and these alkali masses were respectively mixed with the calculated volume of water. This calculation method was implemented for any volume of solution with 12 molarities. The resulting alkaline solution was mixed with a mass of sodium silicate (251.4 g) in a mole ratio of 2.5 to produce the final alkaline solution. The final alkaline solutions were respectively stored in tightly sealed beakers to prevent further absorption of moisture from the environment, and the heat generated by the exothermic reaction of the solution was allowed to dissipate at room temperature for approximately 24 h (Toniolo *et al*. 2017; Durak *et al*. 2021).

The two-component powder formulations were mechanically mixed with a hand mixer in the initially prepared alkaline solution for about 10 min to prepare the geopaste. The desired weight ratio of the alkaline solution to the dry powder mixtures of calcined red clay and powdered glass waste was determined by measuring the viscosity of the geopastes at varying solids loading from 0.5–0.9. The viscosity of the geopastes with different solids loading was measured using a viscometer (RVDE 230, Brookfield Engineering Laboratories, Inc.). The desired ratio of alkali to dry powder mix was then determined according to the ease of workability with the fine aggregates.

Geopolymer Pastes with Varying Fine Aggregates

To determine the amount of river sand to be added, the mass ratios of geopolymer paste to river sand were varied at 1:2.0, 1:2.5, and 1:3.0. For two formulations of geopolymer paste, two particle sizes of river sand and two mass ratios of geopolymer paste to river sand, a total of 12 formulations was obtained, as shown in Table 1. Alphabetical codes were assigned to identify the different variations in the experiment. The addition of river sand to the geopaste was facilitated using a hand mixer for mechanical mixing to homogeneity. The homogenized mixtures of river sand and geopaste were poured into parallelepiped cavity molds for physical characterization. Three molds were made for each experimental condition to represent replications. The rectangular cavity had dimensions of 100 mm x 25 mm x 20 mm, following the previous study (Raki-in *et al.* 2021). A wooden popsicle stick was attached to the outside of the acetate mold with double-sided tape to minimize the sagging and warping of the specimen. After pouring the geoconcrete paste, the molds were covered with an acetate film to protect against cracks due to excessive drying. The cast test bar molds were then placed in a metal chamber by joining two commercially available metal trays (36 cm x 27 cm x 4.0 cm). They were held together and sealed with double-sided foam adhesive and electrical tape, as shown in Appendix Figure II. This heating arrangement was used to avoid excessive drying, which caused severe cracking problems.

Curing Protocol

The filled molds were loaded into a metal enclosure, as shown in Appendix Figure II. The loaded metal enclosure was then placed in a conventional oven heated to 85 °C. The enclosure was then cured at this temperature for 24 h. After heating, the metal housing was removed from the oven and the geo-specimens were stored at ambient conditions for an additional 14 d prior to mold removal and characterizing.

Characterizations of Physical and Mechanical Properties

The tests for the apparent porosity and the water absorption were all performed in accordance with the ASTM C20 standard using boiling water. In this standard test, three replicates of specimens for each condition were boiled for 2 h in a regular kettle with enough water to submerge the specimens. The specimens were then cooled to room temperature while still submerged in water. At room temperature, the specimens were further submerged in water for 24 h before being weighed. The apparent porosity (P) was then evaluated using Equation 2:

$$P, \% = [(W - [d] / (W - S)] \times 100\% \qquad (2)$$

where D is the dry weight before boiling, S is the hanging weight measured while the sample was suspended in a wire mesh hanging from the balance, and W is the saturated mass of the specimen. Similarly, the water absorption (A) was calculated as the percentage of the mass of water absorbed by the specimen to the weight of the dry specimen using Equation 3:

$$P, \% = [(W - [d] / D] \times 100\% \quad (3)$$

The flexural strength was measured according to ASTM C78 for a three-point flexural test. The breaking load for each specimen of test bars was measured using an unconfined compression machine (Marui & Co., Ltd.). This process involved placing a specimen between two points (5 cm apart) or supports and initiating a load using a third point situated between the two points. The load was applied to the center or third point on the specimen, known as the breaking point. The lever was then continuously rotated to move the dial at the top of the machine, which was then continuously rotated until the specimen fractured. The number of lever revolutions was recorded, and the indicated dial load at which the specimen fractured was calculated as in Equation 4:

$$\text{Load, } y = 0.2669 + 0.1809x \quad (4)$$

where y is the applied load (kg) and x represents the number of divisions. Then, after measuring the load, the modulus of rupture was computed using Equation 5:

$$\text{MOR, } \sigma = (3FL) / (2bh^2) \quad (5)$$

where F is the load applied to the sample or the breaking load or the breaking load that is equal to y converted in Newton unit, L is the length between supports (mm), b is the width (mm), and h is the thickness (mm) of the sample. To determine the bulk density (g/cm^3) of the specimens, Equation 6 was used as follows:

$$\rho \text{ (Density)} = M_g / V_g \quad (6)$$

where M_g is the mass of the sample (g), and V_g represents the computed bulk volume. An electronic balance was used to measure the mass of the sample, and the bulk volume was calculated from the measured lateral dimensions of the sample such as length, width, and thickness.

Fabrication of Prototype of the Geoconcrete Roofing Tile

The best formulations that gave the best results in all test parameters were used to produce the roofing tile. Batch samples of the best formulation were prepared. The appropriate mass of geopolymer paste was prepared by adding the required amount of calcined red clay and glass powder to the stock solution of alkali activator with continuous mixing for 4–5 min using a hand mixer. The aggregates were then added in the same proportions and mixing protocol as the test bar specimens. The homogenized concrete mixes were poured into a metal roof tile mold by hand filling and hand pressing with a flat metal sheet. The mold used to form the roof tile was assembled from metal sheets to create a cavity of 270 mm x 170 mm x 18mm, as shown in Appendix Figure III. Petroleum jelly was spread on the inside surfaces of the mold before it was filled with the geoconcrete mixture to facilitate the removal of the solidified product. After filling, the loaded metal mold was cured inside the metal chamber, as per the test bar pieces protocol.

The water penetration test of the formed geoconcrete roof tiles after 14 d of curing at room conditions was evaluated using the sorptivity test adapted from Hall (1989). Both flat faces, two long sides, and one short side of the roof tile were wrapped with plastic adhesive tape to allow unrestricted water movement through the bottom side surface only (unidirectional flow). The sample was first weighed and then submerged in water to a depth of 5 mm with the underside resting on two small metal wires. The tile was held vertically by wooden supports throughout the test period. The time intervals chosen were 5, 10, 30, 60, 120, 180, and 240 min. The time interval was monitored with a stopwatch, then the sample was withdrawn from the water and the excess water was blotted off with a damp cloth. Finally, the weight of the sample was recorded. The cumulative mass gain of the roof tile for every time interval divided by the bottom surface area of the roof tile was plotted against the dipping time to determine the sorptivity coefficient. The sorptivity coefficient (S) is extracted by linear fitting the data using Equation 7:

$$W/\rho A = St^{1/2} + I_o \quad (7)$$

where W is the mass gain (g), A is the surface area tested (mm^2), t is the time interval (min), S is the sorption coefficient ($mm/min^{1/2}$), I_0 is the initial sorption (mm), and ρ is the density of water (g/mm^3).

Statistical Evaluation

A three-factor factorial design was used to characterize the main effects – including glass powder type, solid-to-alkali ratio, and fine sand size – as shown in Table 1. The Analysis of variance (ANOVA) was used to analyze the response characteristics such as bulk porosity, water absorption, bulk density, and flexural strength. The F distribution at the 0.05 significance level was used to determine the significant variations among the main effects, two-factor and three-factor interactions. Depending on the result of the ANOVA analysis, the Duncan multiple range test was used to determine the best conditions for the main effects.

Table 1. Formulations of geopolymer paste and river sand.

Formulation	Geopaste to river sand ratio					
	1:2.0		1:2.5		1:3	
	20-mesh	40-mesh	20-mesh	40-mesh	20-mesh	40-mesh
80% Luinab clay and 20% Tanduay glass powder	A	B	C	D	E	F
80% Luinab clay and 20% Red Horse glass powder	G	H	I	J	K	L

Table 2. Oxide analyses of the aluminosilicate precursors, river sand, and formulations.

Materials/ formulation	SiO_2	Al_2O_3	Fe_2O_3	MgO	CaO	LE	Total	SiO_2/Al_2O_3 molar ratio
Luinab red clay	44.03	14.12	9.58	0.00	0.68	31.58	100.00	5.29
Tanduay bottle	60.07	0.00	1.40	0.00	11.01	27.52	100.00	None
Red Horse bottle	63.61	0.00	0.66	0.00	12.01	23.72	100.00	None
River sand	40.96	9.04	7.93	0.00	4.24	37.82	100.00	7.69
F1 (LRC+10TB)	45.64	12.71	8.77	0.00	1.72	31.17	100.00	6.10
F1 (LRC+15TB)	46.44	12.01	8.36	0.00	2.23	30.97	100.00	6.58
F1 (LRC+20TB)	47.24	11.30	7.95	0.00	2.75	30.76	100.00	7.11
F2 (LRC+10RHB)	45.99	12.71	8.69	0.00	1.82	30.79	100.00	6.15
F2 (LRC+15RHB)	46.97	12.01	8.25	0.00	2.38	30.40	100.00	6.65
F2 (LRC+20RHB)	47.95	11.30	7.80	0.00	2.95	30.00	100.00	7.21

[F1] Luinab red clay with 10–20 wt% Tanduay glass powder; [F2] Luinab red clay with 10–20 wt% Red Horse glass powder

RESULTS AND DISCUSSION

Oxide Analysis and Formulation of Aluminosilicates

Aluminosilicate materials play a crucial role in the reaction with alkaline solutions. The success of this chemical reaction depends on the presence and concentration of oxides such as silica (SiO_2) and alumina (Al_2O_3) in the inorganic precursors. The oxide analyses of the aluminosilicate precursors, together with river sand as the fine aggregate, are shown in Table 2. The precursors used in this study were Luinab clay and waste glass powder from Tanduay and Red Horse bottles. Only the red clay and river sand contained silica, alumina, and other oxides. The glass bottles lacked alumina, as silica is the primary building block of their structures. The glass materials contained a higher silica content, around 60%, compared to red clay and river sand. Meanwhile, light elements such as potassium (K), sodium (Na), lithium (Li), and others were present together in significant amounts.

In the geopolymerization process, the SiO_2/Al_2O_3 ratio is a critical factor in determining the success of the formulated geopaste. The aluminosilicate powders served as a provider of silicate (SiO_4) and aluminate (AlO_4) complexes (Dimas *et al*. 2009) produced by a dissolution process with the alkaline solution. The oxide analyses provide information on the amount of silicon and aluminum ions to be released into the aqueous solution to form the type of aluminosilicate oligomers. Specifically, the ratio of silica to alumina greater than 3 provides sialate-linked oligomers (Cioffi *et al*. 2003) that are readily equilibrated by alkali ions during polymerization. This study used red clay and river sand with molar ratios greater than 5, which are already higher than the fly ash-based composition ranging from 3–4.5 (Dehghani *et al*. 2021). This range of molarity ratios exhibited a better setting of the geopaste to yield desirable mechanical properties. However, increased alumina in the mix can increase porosity, causing reduced strength. It is reasonably desirable to reduce the alumina concentration in the geopaste by adding more silica to create microstructures with low porosity, resulting in improved mechanical properties of the solidified geopolymers (Vafaei and Allahverdi 2017). The increase in silica incorporation suggests that the ratio of silica to alumina in geopolymer blends can be increased without compromising their mechanical properties.

In this study, the ratio of silica to alumina was calculated for some proportions of waste glass addition in powder blends ranging from 0–20%, as shown in Table 2. It is worth noting that the molar ratio of silica to alumina is equivalent to that of red clay when no waste glass is added. The molar ratio was already higher than that of the mixtures based on fly ash. When the waste glass was added to the mixture, the molar ratio of silica to alumina increased to about 7 at the maximum incorporation of waste glass, as shown in Table 2. The closer values of the molar ratios of silica to alumina from both glass wastes were attributed to the similarity of their chemical compositions, which differ only in their minor constituents such as colorants of less than 1%. These molar ratios of silica to alumina in the calculated formulations were considerably higher than those of aluminosilicate mixtures based on fly ash, and the selected proportion of 80 wt% Luinab clay and 20 wt% glass waste was implemented for further experimental investigation in this study. It should be noted that in order to provide an opportunity to recycle the waste at the maximum utilization level, lower additions of waste glass were not experimentally implemented.

Flow Properties of Geopaste with Glass Powder

The flow properties of the geopaste with glass powder are critical for homogeneous mixing with fine sand aggregates. The ratio of alkaline solution to ceramic solids, including glass powder and calcined clay, was achieved at 1:1.25 or 0.8. Ratios lower than this resulted in too fluid geopaste, causing segregation with fine aggregates, whereas higher ratios caused mixing difficulties due to very high viscosity. At this desirable solid ratio in the geopastes, the rheological behavior was graphically presented in Figure 1, which shows a decreasing viscosity with increasing spindle speed. This trend indicates a shear thinning behavior exhibited by all geopastes blended with Tanduay or Red Horse glass powder. The extent of shear thinning of the geopastes was assessed by calculating the ratio as the viscosity reading at 10 revolutions/min divided by that at 60 revolutions/min of the spindle sensor (Gama *et al*. 2019). It was calculated that the extent of shear thinning behavior for the geopaste with Tanduay glass powder was approximately 3.38, which was higher than that for the geopaste with Red Horse glass powder at roughly 2.69. The increase in viscosity for the geopaste with Red Horse glass powder can be attributed to added colorants, which give an amber color.

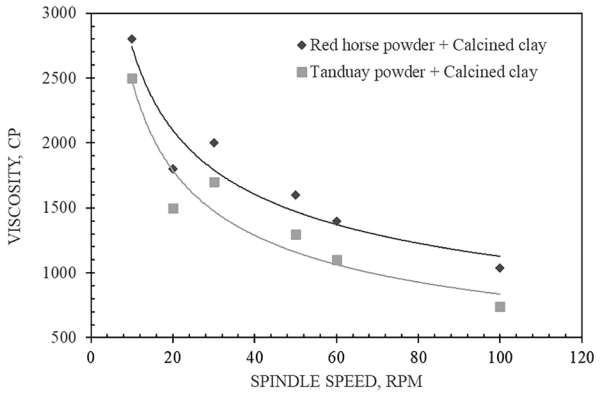

Figure 1. Viscosity profile of geopastes with either red horse glass powder or Tanduay glass powder.

The colorants in container glass can adversely affect the processability of the geopolymer paste because of its sulfide sulfur associated with an iron oxide structure and reducing environment. These glasses are made by melting a glass batch powder with less than 1% by weight of colorants – including iron, sulfate ions, and carbon. The presence of carbon will cause the reduction of the sodium sulfate in the form of a sulfide. Although the transparent glass like the Tanduay bottle had a considerable amount of iron oxide in Table 2, it is believed that the sulfate and carbon were absent in the composition. The amber color of the Red Horse bottle is attributed to the amber pigment. This is a coloring ligand consisting of a central Fe^{3+} ion tetrahedrally coordinated with three oxygen ions O^{2-} and a sulfide of a sulfur ion S^{2-} to form the complex $[Fe^{3+}O_3S^{2-}]^{5-}$ (Morsi *et al*. 2015). Because of this tetrahedral structure with sulfur, the particles of powdered colored glass can be analogous to a sulfide-bearing ore (Basnayaka *et al*. 2017). In aqueous suspension, the sulfide-bearing particles tend to coat or adsorb fine particles of clay minerals, which leads to an unwanted increase in the viscosity of such mineral slurries. The clay mineral particles in red clay can have a platy hexagonal shape with negative faces and positive edges (Swartzen-Allen and Matijevic 1974). These anisotropic surface charges lead to three types of aggregation of clay mineral particles such as edge-to-edge, edge-to-face, and face-to-face aggregation (Rand and Melton 1977). Since the net charge of the tetrahedral chromophore in amber glass is highly negative, the adsorption of clay minerals through their edges onto the surfaces of the glass particles is highly probable. This adsorption scheme results in a voluminous structure that contributes to higher viscosities in the geopolymer paste. Therefore, when preparing a geopolymer paste with container glasses, it is recommended to sort out the colored glasses from the transparent ones to prepare a paste with better processability.

Physical Properties of Geopolymer Paste with Fine Aggregates

The well-mixed geopaste and fine aggregates were heated in the oven for about 24 h and cured at room conditions for approximately 14 d. The resulting parallelepipedal geoconcrete specimens were evaluated for apparent

porosity, an important property used to measure the water-tightness of roofing tiles. This property is the ratio of the volume of open pore space in the specimen to its external volume. The presence of a decreasing concentration of pores in the geoconcrete contributes significantly to the increasing mechanical properties of the material (Hidayati *et al*. 2021). Figure 2 shows the average apparent porosities of cured geoconcrete specimens ranging from 6–20%, depending on the formulations. The size of the fine aggregate, the ratio of the geopaste to fine sand, and

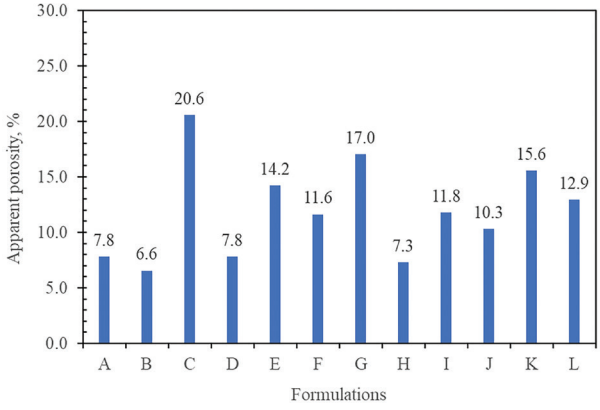

Figure 2. Average apparent porosities of geoconcretes with different formulations.

the type of glass powder contributed to the variation in apparent porosity. This variation was statistically verified by means of the ANOVA table for the three-factorial design in Appendix Table I. At a significance level of 0.05, the geopaste formulation (type of glass powder) and the interaction between geopaste formulation and fine aggregate size were not statistically significant in causing variation in apparent porosity. However, geopaste formulation and its interaction could not be rejected because the three-factor interaction was essentially substantial. The ratio of the geopaste to fine sand, the size of the fine sand aggregates, and their binary interactions were highly significant in reducing the apparent porosities of the geoconcrete samples. This observation could be attributable to the increasing size of the fine aggregate, which provides more void space in the concrete compact (Joseph and Mathew 2012). It is also evident that the ratio of the geopaste to fine sand must be increased to fill the available empty spaces, leading to the reduction of porosity. If the apparent porosity still increases despite increasing the amount of geopaste, it could be inferred that the amount of geopaste added is not sufficient to fill the available empty spaces.

The Duncan multiple range test was used to determine the formulation with the least apparent porosity. As shown in Appendix Table I, the three-factor interaction was highly significant, necessitating a multiple comparison of means on a cell-by-cell basis (Table 1). This statistical analysis resulted in 66 comparisons of apparent porosity means. After a thorough statistical evaluation, Formulations B and H were found to have the lowest apparent porosity of all the other formulations. The average porosity for Formulation B was 6.6%, whereas the average porosity for Formulation H was 7.3%. Although the average porosities were statistically similar for both formulations, the slight difference could be due to the higher viscosity of the geopaste in Formulation H, which could trap more air bubbles during processing and forming. Notably, the measured porosity for Formulation B is closer to the 3–6% range for geopolymer concrete products (Sagoe-Crentsil *et al*. 2014). Both formulations used the finest sand, with the lowest ratio of the geopaste to river sand. Fine sand aggregates allow for a more compact geoconcrete with smaller voids that are adequately filled with the least amount of geopaste. The porosities measured in this study are related to the absorptivity of the formed geopolymer concrete.

Water absorption is one of the critical properties that determine the durability of a concrete roofing tile. A higher water absorption value indicates larger pores within the concrete material, resulting in reduced mechanical strength and durability. The water absorbed by the geo concrete was evaluated using three replicates for each formulation, and the results are shown in Figure 3. The water absorbed by the geo concrete was evaluated using three replicates for each formulation, and the results are shown in Figure 3. It can be observed that there is a considerable variation in the average water absorption for each formulated concrete sample. As the ratio of geopaste to river sand and the particle size of the river sand increase, the water absorption increases. This phenomenon can be attributed to increased voids between larger particles during compaction, which cannot be filled with the available geopaste. The partial filling of void spaces leads

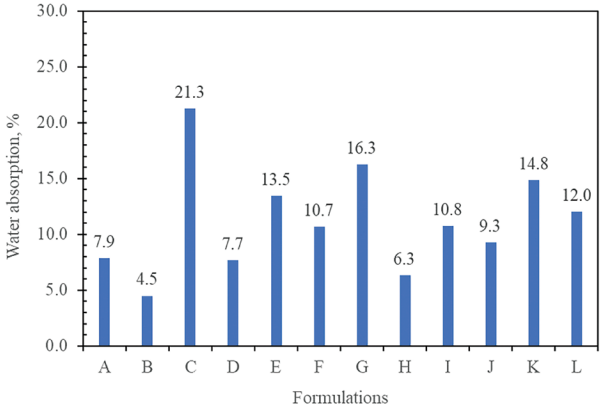

Figure 3. Average water absorption for the different formulations of geoconcrete.

to the aggregation of sand particles during mixing, which traps more air bubbles. Therefore, it is preferable to use finer river sand with the least amount of geopaste added to achieve a minimum water absorption rate.

The ANOVA table for a three-factorial design – as shown in Appendix Table II – confirmed the water absorption variation, consistent with the apparent porosity results discussed earlier. Duncan's multiple range test showed that Formulations B and H consistently had the lowest levels of water absorption in comparison to the other formulations. In contrast, Formulations C and G had the highest water absorption, which is unfavorable for roofing tile applications. According to ASTM C373, porous products can exhibit water absorption in the 9–15% range, whereas the typical water absorption for non-porous tiles is 0.1–0.5%. As a result, the water absorption of Formulations B and H falls between porous and non-porous products. Notably, Formulations B and H were optimal for the concrete tile application.

The bulk density of the geoconcrete determines the heaviness of roofing materials used in construction. While concrete-based materials are typically expected to have higher bulk densities, this property can offer several benefits in energy efficiency, durability, and longevity. Higher bulk density also translates into superior mechanical strength, critical for better resistance to harsh weather conditions. Therefore, the bulk densities of the geoconcrete specimens formed in this study were characterized and plotted, as shown in Figure 4. Interestingly, all the measured bulk densities were found to be below the range of bulk densities for common geopolymeric materials (Mohammed and Hama 2014), which are typically between 1.20–1.80 g/cm^3. Thus, the geoconcrete materials in this study can be considered lightweight roofing materials. The variation of bulk densities among the different formulations was evaluated using an ANOVA table for a three-factor factorial design, as shown in Appendix Table III. The statistical results

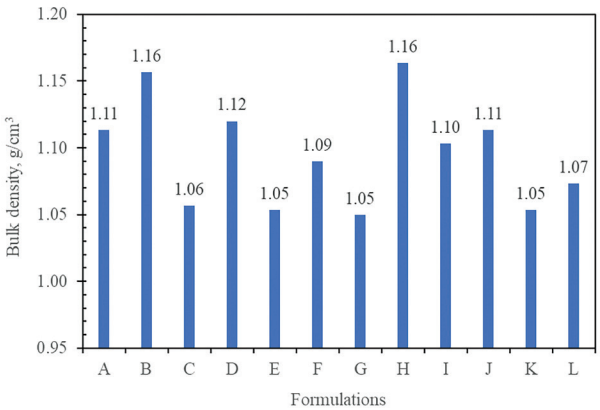

Figure 4. The average bulk densities of all geoconcrete formulations.

indicated that only the size of the fine sand and the ratio of geopaste to fine sand strongly affected the observed bulk densities.

A Duncan multiple range test was performed to determine the optimal geopaste-to-sand ratio and fine aggregate size. The multiple means comparisons showed that formulations B and H consistently had the highest bulk densities of approximately 1.16 g/cm^3. This result is consistent with the previously discussed findings of these two formulations having the lowest porosity and water absorption. Therefore, finer sand particles should be used with the lowest amount of geopaste to achieve a higher bulk density while maintaining a lightweight roofing material.

Flexural strength is critical for geopolymer concrete tiles, as it measures the material's resistance to bending in high winds after installation. The measured flexural strengths of the different geoconcrete formulations are shown in Figure 5. It can be observed that all formulations have the same flexural strengths except formulations A, B, and H, which have higher values. This finding was verified by ANOVA through a three-factorial design, and the results were presented in Appendix Table IV. Statistically, only the ratio of geopaste to a fine sand size significantly

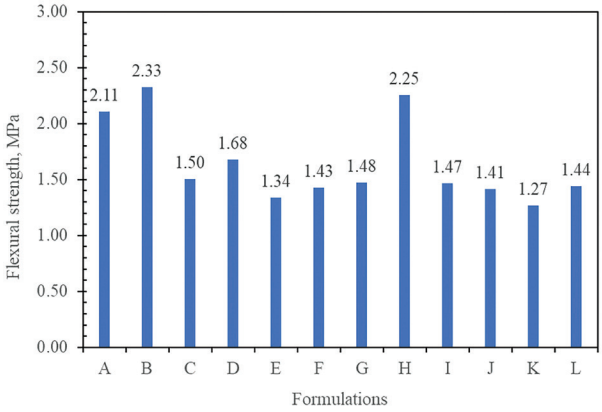

Figure 5. The average flexural strengths of all geoconcrete formulations.

affected flexural strength. This finding is expected because the geopaste acts as a binder between the particles and fills voids, providing improved mechanical support after setting. As reported in previous studies, the flexural strengths of all formulations in this study fall within the range of 1.3–3.50 MPa for standard geopolymer products (Sagoe-Crentsil *et al*. 2014). For structural applications, the flexural strength of the geopolymer concrete must be greater than 3 MPa. Formulations B and H were found to have the highest flexural strengths through a Duncan multiple range test with multiple comparisons of means at a significance level of 0.05. Formulation B

exhibited a flexural strength of 2.33 MPa, slightly higher than formulation H at approximately 2.25 MPa. Both formulations had similar flexural strengths, as confirmed by statistical analysis. Furthermore, as previously discussed, these two formulations demonstrated the lowest porosity and water absorption, as well as the highest bulk density.

Prototype of the Geopolymer Concrete Roof Tile

As described above, Formulations B and H displayed favorable physical properties – including low apparent porosity (6.6–7.3%), low water absorption (4.5–6.3%), high bulk density (1.16 g/cm^3), and high flexural strength (2.33–2.25 MPa). These results demonstrate the notable quality of these formulations. The formulations consisted of geopolymer paste with 20% glass powder (either Tanduay or Red Horse) and fine aggregates (passing 40 mesh and retained on 60 mesh) at a 1:2 ratio of geopolymer paste to sand. The roofing tiles prototypes were confidently created using the geopolymer concrete mixes, as illustrated in Appendix Figure IV. The mixes underwent a heating process in an oven at 80 °C and were cured at room temperature for approximately 14 d. The addition of smaller particles of river sand gave the tiles a finer texture and a rich brown color. It is recommended to use smaller particles of river sand in the mix to achieve a more attractive appearance. In addition, the aesthetic qualities of the tiles can be enhanced by adding an extra coating material.

The prototypes were fabricated to meet the standard weight requirements for residential construction, typically between 46.4–58.6 kg/m^2 for concrete roof tiles. Lightweight roof tiles weighing between 26.9–34.2 kg/m^2 are also available from various manufacturers for areas where weight is a concern (Martin 2001). In this study, the weight of the geopolymer concrete tile was measured to be 1.12 kg in an area of 0.046 m^2. This is equivalent to 24.25 kg/m^2. The manufactured geopolymer concrete tile weighed approximately 1.21 kg for the volume dimensions of 270 mm x 170 mm x 18 mm, making it suitable for use as a lightweight roofing material using river sand in the concrete mix.

The water penetration performance of the geopolymer concrete prototypes was evaluated in terms of the water sorption coefficient. This coefficient measures the ease of water entry into unsaturated geopolymer concrete pores through capillary suction. The fluid entry depends on the accessible apparent porosities – including interconnected pores, pore tortuosity, and pore channel volumes (Moore *et al*. 2020). The fluid completely penetrates and fills all available pore volumes connected to the surfaces, which accounts for the mass gain of the roof tile sample. The geopolymer concrete bodies formed with Tanduay and Red Horse glass powders exhibit measured apparent porosities of 6.6 and 7.3%, respectively. The sorptivity coefficients of the two concrete samples were significantly different, as demonstrated in Figure 6, despite their values not showing a significant difference. The plot in Figure 6 shows a linear trend of increased liquid sorption with increasing square root of time. These findings confidently support the conclusion that porosity plays a crucial role in the sorption behavior of concrete. Additionally, the figure illustrates that a slight decrease in the apparent porosity results in a significant reduction in the amount of water sorbed. The sorptivity coefficient of roof tiles made from Red Horse glass powder was determined to be 0.2653 mm/

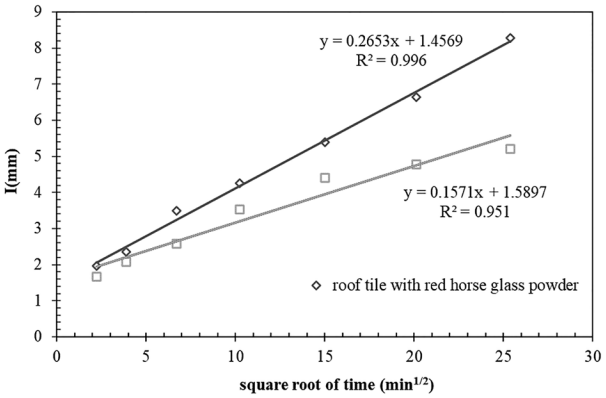

Figure 6. The capillary absorption rates of geopolymer concrete roof tiles with Tanduay and Red Horse glass powders.

min$^{1/2}$, whereas for roof tiles made from Tanduay glass powder, the value was reduced to 0.1571 mm/min$^{1/2}$. It is worth noting that sorption coefficients for cement-based concrete typically range from 0.094–0.170 mm/min$^{1/2}$ (Hall 1989). Concrete roof tiles must have sorptivity values below 0.20 mm/min$^{1/2}$ to maintain tightness and resist liquid permeation. The geopolymer concrete roof tile with Tanduay glass powder is in compliance with this requirement and is a promising material to be used in the construction of roof tiles.

CONCLUSION

The production of a concrete roof tile is successfully demonstrated using the red clay-based geopolymer pastes with powdered transparent and colored container glasses and river sand as a concrete filler. Specifically, a high shear thinning behavior of the geopaste with the transparent glass powder was observed using a solid-to-alkali solution ratio of about 0.80. The best ratio of the geopaste to fine aggregate is 1:2, giving a maximum mechanical strength of 2.33 MPa with an apparent porosity of 6.30% and water absorption of 4.50%. The bulk density of the concrete

block is approximately 1.16 g/cm^3, which is classified as a lightweight material. Finally, the manufactured prototype of the geopolymer concrete block has the lowest sorption coefficient of 0.170 mm/min$^{1/2}$. This measured sorption coefficient, together with the physical properties, indicates that the produced roof tile is a potential building material.

ACKNOWLEDGMENTS

The authors would like to thank Miss Raizza Marie E. Rivas for carrying out the water sorption test and the faculty and staff of the Department of Materials and Resources Engineering and Technology of Mindanao State University–Iligan Institute of Technology for allowing the authors to carry out the study in their laboratory.

STATEMENT ON CONFLICT OF INTEREST

The authors certify that they have no relationship to or participation in any organization or agency that may have a competing financial interest in the subject matter or materials discussed in this paper.

REFERENCES

ALOUANI MEL, ALEHYEN S, ACHOURI MEL, HAJJAJI A, ENNAWAOUI C, M'HAMED TAIBI M. 2020. Influence of the Nature and Rate of Alkaline Activator on the Physicochemical Properties of Fly Ash-Based Geopolymers. Adv Civ Eng 2020: 1–13.

[ASTM] American Society for Testing and Materials. 2010. Standard Test Methods for Apparent Porosity, Water Absorption, Apparent Specific Gravity, and Bulk Density of Burned Refractory Brick and Shapes by Boiling Water [C20]. West Conshohocken PA: ASTM International.

[ASTM] American Society for Testing and Materials. 2002. Standard test method for flexural strength of concrete using simple beam with third-point loading [C78]. West Conshohocken, PA: ASTM International.

[ASTM] American Society for Testing and Materials. 2018. Standard Test Methods for Determination of Water Absorption and Associated Properties by Vacuum Method for Pressed Ceramic Tiles and Glass Tiles and Boil Method for Extruded Ceramic Tiles and Non-tile Fired Ceramic Whiteware Products [C373]. West Conshohocken, PA: ASTM International.

BASNAYAKA L, SUBASINGHE N, ALBIJANIC B. 2017. Influence of clays on the slurry rheology and flotation of a pyritic gold ore. Appl Clay Sci 136: 230–238.

CHINDAPRASIRT P, DE SILVA P, SAGOE-CRENTSIL K, HANJITSUWAN S. 2012. Effect of SiO_2 and Al_2O_3 on the setting and hardening of high calcium fly ash-based geopolymer systems. J Mater Sci 47: 4876.

CIOFFI R, MAFFUCCI L, SANTORO L. 2003. Optimization of geopolymer synthesis by calcination and polycondensation of a kaolinitic residue. Resour Conserv Recycl 40: 27.

CONRADT R. 2008. Chemical durability of oxide glasses in aqueous solutions: a review. J Am Ceram Soc 91(3): 728–735.

DEHGHANI A, ASLANI F, PANAH NG. 2021. Effects of initial SiO_2/Al_2O_3 molar ratio and slag on fly ash-based ambient cured geopolymer properties. Constr Build Mater 293: 123527.

DIMAS D, GIANNOPOULOU I, PANIAS D. 2009. Polymerization in sodium silicate solutions: a fundamental process in geopolymerization technology. J Mater Sci 44: 3719–3730.

DOUGLAS RW, EL-SHAMY TMM. 1967. Reactions of Glasses with Aqueous Solutions. J Am Ceram Soc 50(1): 1–8.

DURAK U, İLKENTAPAR S, KARAHAN O, UZAL B, ATIŞ CD. 2021. A new parameter influencing the reaction kinetics and properties of fly ash based geopolymers: a pre-rest period before heat curing. J Build Eng 35: 102023.

GAMA AP, HUNG YC, ADHIKARI K. 2019. Optimization of Emulsifier and Stabilizer Concentrations in a Model Peanut-Based Beverage System: a Mixture Design Approach. Foods 8(4): 116.

ESSAIDI N, SAMET B, BAKLOUTI S, ROSSIGNOL S. 2014. Feasibility of producing geopolymers from two different Tunisian clays before and after calcination at various temperatures. Appl Clay Sci 88–89: 221–227.

GAO X, YAO X, XIE R, LI X, CHENG J, YANG T. 2022. Performance of fly ash-based geopolymer mortars with waste cathode ray tubes glass fine aggregate: a comparative study with cement mortars. Constr Build Mater 344: 128243.

GOTO KJ. 1955. States of silica in aqueous solution. II. Solubility of amorphous silica. J Ceram Soc Jpn 76: 1364–1366.

HALL C. 1989. Water sorptivity of mortars and concretes: a review. Mag Concr Res 41(147): 51–61.

HAMZAH HK, HUSEIEN GF, ASAAD MA, GEORGESCU DP, GHOSHAL SK, ALRSHOUDI F. 2021. Effect of waste glass bottles-derived nanopowder as slag replacement on mortars with alkali activation: durability characteristics. Case Stud Constr Mater 15: e00775.

HENAO RIOS LM, HOYOS TRIVIÑO AF, VILLAQUIRÁN-CAICEDO MA, MEJÍA DE GUTIÉRREZ R. 2023. Effect of the use of waste glass (as precursor, and alkali activator) in the manufacture of geopolymer rendering mortars and architectural tiles. Constr Build Mater 363: 129760.

HIDAYATI RE, FARADILLA FS, NURKHOLIFAH R, NURLINA Y, BAYUAJI R, HARTANTO D, PRASETYOKO D, FANSURI H. 2021. The effect of water glass source variation on the mechanical properties of fly ash-based geopolymer. AIP Conference Proceedings: Green Design and Manufacture 2339(1): 020046.

JOSEPH B, MATHEW G. 2012. Influence of aggregate content on the behavior of fly ash based geopolymer concrete. Sci Iran 19(5): 1188–1194.

KAI MF, DAI JG. 2021. Understanding geopolymer binder-aggregate interfacial characteristics at molecular level. Cem Concr Res 149: 106582.

LO KW, LIN KL, CHENG TW, SHIU HS. 2018. Effect of alkali activation thin film transistor-liquid crystal display waste glass on the mechanical behavior of geopolymers. Constr Build Mater 162: 724–731.

MANIKANDAN P, VASUGI V. 2022. Potential utilization of waste glass powder as a precursor material in synthesizing ecofriendly ternary blended geopolymer matrix. J Clean Prod 355: 131860.

MARAGHECHI H, MARAGHECHI M, RAJABIPOUR F, PANTANO CG. 2014. Pozzolanic reactivity of recycled glass powder at elevated temperatures: reaction stoichiometry, reaction products, and effect of alkali activation. Cem Concr Compos 53: 105–114.

MARTIN F. 2001. Roofing with Concrete Tile. J Light Constr Retrieved on 29 Apr 2023 from https://www.jlconline.com/how-to/roofing/roofing-with-concrete-tile-1_o

MARTÍNEZ-MARTÍNEZ S, PÉREZ-VILLAREJO L, DOLORES ELICHE-QUESADA D, SÁNCHEZ-SOTO PJ. 2023. New Types and Dosages for the Manufacture of Low-energy Cements from Raw Materials and Industrial Waste under the Principles of the Circular Economy and Low-carbon Economy. Mater 16(2): 802–837.

MOHAMMED JH, HAMA AJ. 2014. Materials, properties, and application review of lightweight concrete. Rev Téc Ing Univ Zulia 37(2): 10–15.

MOORE A, BAKERA AT, ALEXANDER M. 2020. Water Sorptivity and Porosity Testing of Concrete. Tech Rep, Vol. 162. DOI: 10.13140/RG.2.2.21185.07525

MORSI MM, EL-SHERBINY SI, MOHAMED KM. 2015. Spectroscopic investigation of amber color silicate glasses and factors affecting the amber related absorption bands. Spectrochim Acta A Mol Biomol Spectrosc 145: 376–383.

MORSY MS, ALSAYED SH, AL-SALLOUM Y, ALMUSALLAM T. 2014. Effect of Sodium Silicate to Sodium Hydroxide Ratios on Strength and Microstructure of Fly Ash Geopolymer Binder. Arab J Sci Eng 39: 4333–4339.

NOVAIS RM, ASCENSÃO G, SEABRA MP, LABRINCHA JA. 2016. Waste glass from end-of-life fluorescent lamps as raw material in geopolymers. Waste Manag 52: 245–255.

QIN Y, HE Y, WU B, MA S, ZHANG X. 2017. Regulating top albedo and bottom emissivity of concrete roof tiles for reducing building heat gains. Energy Build 156: 218–224.

RAKI-IN JM, VILLAGRACIA JR KLM, MENCHAVEZ RL. 2021. Fabrication of a Wall-panel Board Using Rice Husk and Red Clay-based Geopolymer. Mindanao J Sci Technol 19(1): 250–268.

RAND B, MELTON IE. 1977. Particle interactions in aqueous kaolinite suspensions: I. Effect of pH and electrolyte upon the mode of particle interaction in homoionicsodium kaolinite suspensions. J Colloid Interface Sci 60(2): 308–320.

REHMAN SKU, IMTIAZ LI, FAHID ASLAM F, KHAN MK, MUHAMMAD HASEEB M, JAVED MF, ALYOUSEF R, ALABDULJABBAR H. 2020. Experimental Investigation of NaOH and KOH Mixture in SCBA-based Geopolymer Cement Composite. Mater (Basel) 13(15): 3437–3465.

RIDTIRUD C, CHINDAPRASIRT P. 2019. Properties of Lightweight Aerated Geopolymer Synthesis from High Calcium Fly Ash and Aluminum Powder. Int J GEOMATE 16(57): 67–75.

SAGOE-CRENTSIL KK, YAN S, GESTHUIZEN L. 2014. Geopolymer product [US20140238273A1].

SHILAR FA, GANACHARI SV, PATIL VB, ALMAKAYEEL N, KHAN TMY. 2023. Development and optimization of an eco-friendly geopolymer brick production process for sustainable masonry

construction. Case Stud Constr Mater 18: e02133.

SHILAR FA, GANACHARI SV, PATIL VB, JAVED S, KHAN TMY, BAIG RU. 2022. Assessment of Destructive and Nondestructive Analysis for GGBS Based Geopolymer Concrete and Its Statistical Analysis. Polymers 14: 3132.

SIDDIKA A, HAJIMOHAMMADI A, FERDOUS W, SAHAJWALLA V. 2021. Roles of Waste Glass and the Effect of Process Parameters on the Properties of Sustainable Cement and Geopolymer Concrete – a State-of-the-Art Review. Polym 13(22): 3935.

SINGH B, ISHWARYA G, GUPTA M, BHATTACHARYYA SK. 2015. Geopolymer concrete: a review of some recent developments. Constr Build Mater 85: 78–90.

SWARTZEN-ALLEN SL, MATIJEVIC E. 1974. Surface and colloid chemistry of clays. Chem Rev 74(3): 385–400.

TONIOLO N, TAVERI G, HURLE K, ROETHER JA, ERCOLE P, DLOUHÝ I, BOCCACCINI AR. 2017. Fly-ash-based Geopolymers: How the Addition of Recycled Glass or Red Mud Waste Influences the Structural and Mechanical Properties. J Ceram Sci Technol 8(3): 411–420.

VAFAEI M, ALLAHVERDI A. 2017. High strength geopolymer binder based on waste-glass powder. Adv Powder Technol 28(1): 215–222.

VAFAEI M, ALLAHVERDI A, DONG P, BASSIM N, MAHINROOST M. 2021. Resistance of red clay brick waste/phosphorus slag-based geopolymer mortar to acid solutions of mild concentration. J Build Eng 34: 102066.

APPENDICES

Table I. ANOVA analysis of porosities for different geoconcrete formulations.

Source of variation	Sum of squares	Degrees of freedom	Mean square	F_o	F_{stat}	Values	Comments
Geopaste formulations (A)	10.028	1	10.028	2.634	0.05, 1, 24	4.26	Not significant
Geopaste to river sand ratio (B)	99.260	2	49.630	13.037	0.05, 2, 24	3.4	Significant
Fine sand sizes (C)	231.040	1	231.040	60.689	0.05, 1, 24	4.26	Significant
AB	100.389	2	50.194	13.185	0.05, 2, 24	3.4	Significant
AC	1.868	1	1.868	0.491	0.05, 1, 24	4.26	Not significant
BC	31.547	2	15.773	4.143	0.05, 2, 24	3.4	Significant
ABC	147.102	2	73.551	19.320	0.05, 2, 24	3.4	Significant
Error	91.367	24	3.807				
Total	**712.600**	**35**					

Table II. ANOVA analysis of water absorption for the different geoconcrete formulations.

Source of variation	Sum of squares	Degrees of freedom	Mean square	F_o	F_{stat}	Values	Comments
Geopaste formulation (A)	4.168	1	4.168	0.991	0.05, 1, 24	4.26	Not significant
Geopaste to river sand ratio (B)	114.853	2	57.426	13.659	0.05, 2, 24	3.4	Significant
Fine sand sizes (C)	289.283	1	289.283	68.808	0.05, 1, 24	4.26	Significant
AB	138.683	2	69.342	16.493	0.05, 2, 24	3.4	Significant
AC	7.517	1	7.517	1.788	0.05, 1, 24	4.26	Not significant
BC	38.244	2	19.122	4.548	0.05, 2, 24	3.4	Significant
ABC	135.126	2	67.563	16.070	0.05, 2, 24	3.4	Significant
Error	100.902	24	4.204				
Total	**828.777**	**35**					

Table III. ANOVA analysis of the bulk densities of different geoconcrete formulations.

Source of variation	Sum of squares	Degrees of freedom	Mean square	F_o	F_{stat}	Values	Comments
Geopaste formulations (A)	0.0003	1	0.0003	0.127	0.05, 1, 24	4.26	Not significant
Geopaste to river sand ratio (B)	0.0172	2	0.0086	3.940	0.05, 2, 24	3.4	Significant
Fine sand sizes (C)	0.0205	1	0.0205	9.410	0.05, 1, 24	4.26	Significant
AB	0.0035	2	0.0018	0.810	0.05, 2, 24	3.4	Not significant
AC	0.0000	1	0.0000	0.000	0.05, 1, 24	4.26	Not significant
BC	0.0043	2	0.0022	0.986	0.05, 2, 24	3.4	Not significant
ABC	0.0060	2	0.0030	1.378	0.05, 2, 24	3.4	Not significant
Error	0.0524	24	0.0022				
Total	**0.1043**	**35**					

Table IV. ANOVA analysis of flexural strengths for the different geoconcrete formulations.

Source of variation	Sum of squares	Degrees of freedom	Mean square	F_o	F_{stat}	Values	Comments
Geopaste formulation (A)	0.284	1	0.284	0.837	0.05, 1, 24	4.26	Not significant
Geopaste to river sand ratio (B)	2.997	2	1.499	4.420	0.05, 2, 24	3.4	Significant
Fine sand sizes (C)	0.475	1	0.475	1.402	0.05, 1, 24	4.26	Not significant
AB	0.161	2	0.081	0.238	0.05, 2, 24	3.4	Not significant
AC	0.044	1	0.044	0.129	0.05, 1, 24	4.26	Not significant
BC	0.329	2	0.165	0.485	0.05, 2, 24	3.4	Not significant
ABC	0.237	2	0.118	0.349	0.05, 2, 24	3.4	Not significant
Error	8.137	24	0.339				
Total	**12.665**	**35**					

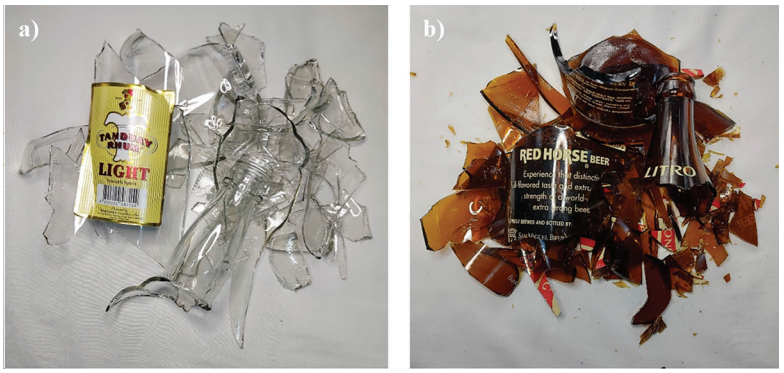

Figure I. Container waste bottles: [a] broken Tanduay rhum and [b] broken Red Horse beer.

Figure II. Metallic chamber as an enclosure for heating geoconcrete cast.

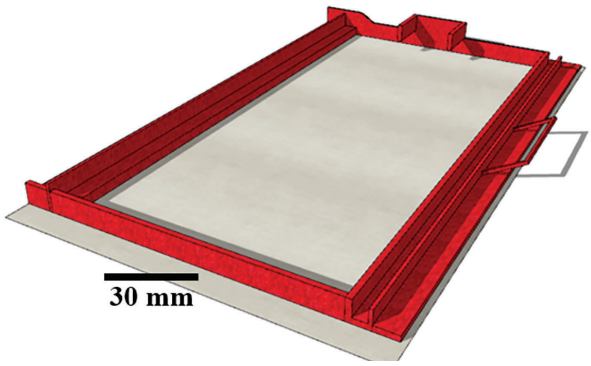

Figure III. The metal mold design for the geoconcrete roofing tile.

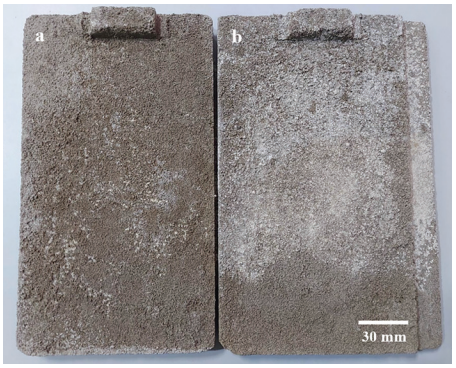

Figure IV. Prototype of the geopolymer roof tiles made with geopastes of [a] Tanduay glass powder and [b] Red Horse glass powder, with river sand as fine aggregate.